UNIVERSITY OF TARTU

FACULTY OF SCIENCE AND TECHNOLOGY

INSTITUTE OF PHYSICS

Magnus Mets

MECHANICAL CHARACTERIZATION OF

SILVER NANOWIRES

Bachelor Thesis (12 EAP)

Supervisors: Sergei Vlassov, PhD

Approved for defence ....

Supervisors ....

signature, date

Tartu 2012

Table of contents

Abbreviations

AFM	Atomic Force Microscope
EBID	Electron-Beam-Induced Deposition
FCC	Face-Centered Cubic
FIB	Focused Ion Beam
NEMS	Nanoelectromechanical Systems
NW	Nanowire
QTF	Quartz Tuning Fork
SEM	Scanning Electron Microscope
TEM	Transmission Electron Microscope
VLS	Vapor-Liquid-Solid

1. Introduction

Every material has a set of intensive properties, like e.g. electrical resistance or mechanical strength, which stay constant while the physical dimensions may change. But it is true only for macroscopic objects. If the material's dimensions are approaching nanometer size then the properties and the behavior of this nano object are quite different from that of micro or macro object. This phenomenon is called size effect. Moreover the properties of nanoscopic material are size dependent [1] and therefore can be controlled with great precision. This phenomenon can be used to improve overall characteristics of various devices and to make them more efficient. In order to do so we need to know essential properties of nanoscopic materials. However, due to their small size measuring of these properties is not trivial and requires specific methods and experience.

One of the most promising materials for future technologies is nanostructured silver (Ag), in particular Ag nanowires (NWs), due to their excellent electrical and thermal conductivity [2, 3], perfect structure and ease of synthesis. In certain applications, like e.g. flexible transparent electrodes [4], nanoswitches [5], and resonators [6], Ag NWs are required to withstand numerous repetitive deformations. Ag NWs have also potential in nanophotonics [7], where significant bending is required to guide the light in desired direction. Defects introduced by bending may strongly affect light propagation in waveguides [7, 8]. Therefore deeper understanding of elasticity, plasticity, fatigue and fracture of Ag NWs is essential for performance and reliability of above devices.

Commonly Ag NWs have pentagonal symmetry where five regular crystalline domains are divided by twin boundaries [9]. Such structure leads to intrinsic elastic strains that may result in mechanical properties significantly different from those of bulk Ag.

There are several methods reported on mechanical characterization of pentagonal Ag NWs, namely, three point bending test [10, 11, 12], tensile test [1], and nanoindentation [13]. Although these methods cover a wide range of mechanical properties, results cannot be extended to all types of deformation due to the fact that moduli and strengths of crystalline anisotropic materials depend on test conditions. Listed methods do not include important case of pure bending taking place in some NEMS and nanoplasmonics applications. Therefore it is evident that additional study of Ag NW deformation is required to improve our understanding of Ag NW properties and behavior and assure the functionality and the reliability of Ag NW-based systems.

The present thesis is dedicated to mechanical characterization of chemically synthesized Ag NWs. In the first part of the thesis synthesis, structure and known properties of Ag NWs are described. Overview of common techniques for mechanical testing of 1D structures is given. In

the second part of the thesis original work on mechanical characterization of Ag NWs by advanced cantilevered beam-bending technique, in which pure bending conditions are realized, is reported. Experiments were performed inside scanning electron microscope using 3D nanopositioner and self-made force sensor. Elastic beam theory was implemented to extract Young's modulus and yield strength. Moreover, fatigue test were performed, where NW was cyclically bent multiple times. The present method has never been used for mechanical characterization of Ag NWs before.

2. Background

2.1 Introduction to nanowires

Nanowires (NWs) are high aspect ratio nanostructures with diameter ranging from few nanometers to few hundred nanometers. NWs with small aspect ratio (3-5) are also called nanorods. There exist a number of types of NWs, mainly metallic (e.g., Au, Ag, W etc.), semiconductor (e.g., Si, InAs, GaN, ZnO), and insulating (e.g., TiO_2, SiO_2).

Due to their very small size NWs have significantly different, and often even superior properties compared to bulk objects made out of the same material [14]. NWs have increased surface-to-volume ratio, enhanced exciton binding energy, diameter-dependent band gap, increased surface scattering for electrons and phonons, and other peculiarities. Unlike other low-dimensional systems NW have two quantum confined directions, leaving one unconfined direction for electrical conduction. Hence the other name, quantum wire. [15]

NWs have many promising applications in nanotechnology including high-density data storage, electronic and opto-electronic nanodevices, metallic interconnects, nanoelectromechanical systems and others [16, 17]. Applying NWs in various devices and systems would help in the further miniaturization process that could decrease their energy consumption along with increasing their efficiency, like has happened with the microprocessor. One of the greatest advantage of NWs from an applicative point of view is that in contrast to their bulk counterparts, some of the materials parameters, like e.g. thermal conductivity, which are critical for certain applications, can be independently controlled and even NWs made of the same material may possess different properties due to differences in their crystal phase, crystalline size, surface conditions, and aspect ratios, which depend on the synthesis methods and conditions used in their preparation [15].

2.2 Synthesis

The basis of one dimensional nanostructure formation is about crystallization. The evolution of a solid from a vapor, liquid, or solid phase comprises of two fundamental steps: nucleation and growth. As the concentration of the ingredients (atoms, ions, or molecules) of solid becomes sufficiently high, they aggregate into small clusters (or nuclei) through homogeneous nucleation. With continuous supply of the ingredients, these nuclei can serve as seeds for further growth to form larger structures. [16]

The following is a brief overview of some main synthesis methods for NWs.

2.2.1 Vapor-liquid-solid process

A general vapor-liquid-solid (VLS) process starts with the dissolution of gaseous reactants into nanosized liquid droplets of metal, which are the catalyst in this process, followed by nucleation and growth of single-crystalline rods and then wires. The one dimensional growth is mainly caused and dictated by the liquid metal droplets. The size of these droplets stay essentially unchanged during the entire process of wire growth. Due to this fact, every droplet limits the lateral growth of individual NW. As a very important requirement, there should be good solvent, that could form liquid alloys with the target material, ideally eutectic compounds. All the essential steps of this method are schematically illustrated in figure 1. VLS process has become a widely used method for synthesizing one dimensional nanostructures from wide array of inorganic materials. But this method has also some challenges, the biggest one is the selection of an appropriate catalyst that will work with the solid material to be processed into nanostructures. [16]
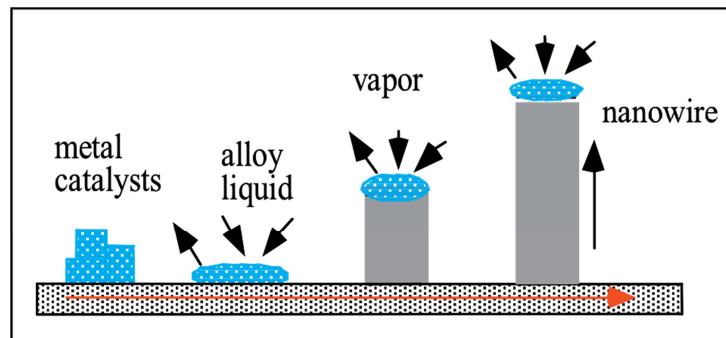

Figure 1. Schematic illustration showing the growth of a NW via the vapor-liquid-solid mechanism. [17]

2.2.2 Solution-liquid-solid method

Solution-liquid-solid method is an analogue to the VLS process that has been developed to synthesis highly crystalline NWs of III-V semiconductors at relatively low temperatures. In a typical process, a metal (e.g., In, Sn, or Bi) with a low melting point is used as the catalyst and the wanted material is generated through the decomposition of organometallic precursors. The product is basically single-crystalline whiskers or filaments with lateral dimensions of 10-150 nm and lengths up to several micrometers. [16]
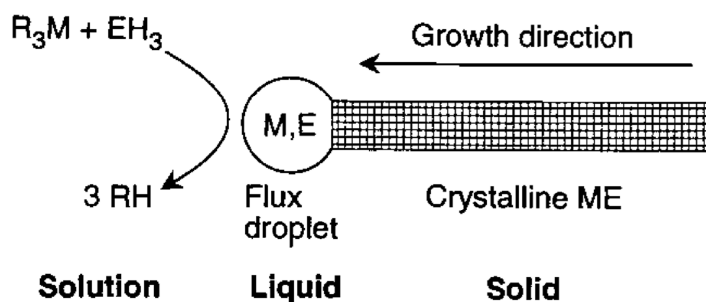
Figure 2. Schematic illustration showing the growth of a NW through the solution-liquid-solid mechanism. M and E are elements of the III-V semiconductor. [18]

2.2.3 Solvothermal method

Solvothermal synthesis uses a solvent under pressures and temperatures above its critical point to increase the solubility of a solid and to speed up reactions between solids. In a usual procedure, a precursors and possibly a reagent (such as amines) capable of regulating the crystal growth are added into a solvent with appropriate ratios. Then this mixture is placed in an autoclave to allow the reaction and NW growth to proceed at elevated temperatures and pressures. The main advantage of this approach is that most materials can be made soluble in a proper solvent by heating and pressurizing the system close to its critical point. Therefore this method should be well suited for any solid material. This procedure has been extensively used to process rich variety of materials into wires, tubes, and whiskers. Although this method seems to be versatile in producing one dimensional nanostructures, the products were often characterized by low yield, low purity, and poor uniformity in size or morphology. [16]

2.2.4 Solution-phase method

The present method is based on nucleation and anisotropic growth of the NWs in solution. This method can produce one dimensional nanostructures from a great variety of materials. Advantage of solution phase synthesis is that it is possible to produce large quantities of nanostructures. Polyol synthesis is one of this method's subtype. This synthesis involves heating a polyol with salt precursor and a polymeric capping agent to produce metal colloids. For example silver (Ag) NWs are synthesized by reducing $AgNO_3$ with ethylene glycol in the presence of polyvinyl pyrrolidone, which is the capping agent. By carefully controlling the synthesis conditions pentagonal Ag NWs can be obtained. [1, 2]

2.3. Silver nanowires

2.3.1 Silver

Ag is one of the oldest metal known to mankind, due to fact that it is chemically inert. It does not react with oxygen under normal conditions, but does slowly react with sulfur compounds in the air. The result of this reaction can be seen as a tarnish on silverware. Ag has a melting point of 961.93 °C and relatively high density of 10.492 g/cm^3, at 20 °C [19]. Ag has face-centered cubic (FCC) crystal structure. It is a very ductile metal. Among metals, Ag has the lowest electrical resistance and highest thermal conductivity, 0.01629 μΩ·m (27 °C) and 4.29 W/(cm·K) (27 °C) respectively. Also Ag is a diamagnetic material. Despite the excellent electrical and thermal properties, its high cost limits Ag from being widely used in macroscale applications. [20]

2.3.2 Structure of silver nanowires

Ag NWs synthesized by polyol reduction in the presents of PVP have pentagonal structure [9, 21, 22]. Ag NW's axis is in the [110] direction, tips of the NW are capped by ten {111} planes and bounded by five {100} planes [21]. Transmission electron microscopy (TEM) studies of Ag NW's cross-section show presents of five-twinned structure [9]. Selected area electron diffraction patterns obtained from the Ag NW's cross-section show remarkable fivefold symmetry and that the Ag NW consists of 5 FCC subcrystals with [110] orientation [9]. These monocrystals are joined together along a common [110] edge and along {111} faces [21]. Due to fact that the angle between two FCC {111} planes is roughly 70.5° there occurs an angular gap of 7.4°. Since Ag NWs have a closed structure and the angular gaps are not present, and if one assumes that monocrystalline regions preserve FCC crystal lattice, NWs must be strained in order to eliminate the angular gaps. The procedure of elimination of angular gaps by rotations of gap faces is equivalent to the introducing a disclination defect into the crystal. Disclination is a linear defect in solid materials. It is a rotational displacement and is characterized by vector ω, called Frank's vector. In the case of pentagonal Ag NWs the distortion is wedge disclination. [23]

This structure of Ag NW leads to the presence of intrinsic elastic strain that in turn promotes various mechanisms of stress relaxation like stacking faults [24]. Figure 3b shows high- resolution TEM image, where lattice fringes within Ag subcrystals and near the boundaries can be clearly seen. The appearance of anomalous contrast fringes in the subcrystals suggests the presence of a high density of stacking faults in addition to the twin boundaries. It should be

mentioned that some twin boundaries are very sharp and result in a well-defined twin relationship between the twinned subcrystals. But at the same time, a large fraction of the boundaries induces a very complex contrast with evident structural distortions, especially at the core area of the NW. [9]

According to Chen et al. observations, the 7.4° gap occurring in a pentagonal rod is shared by three twin boundaries. They proposed a model for the cross-section of fivefold twinned nanorods based on their experimental results, where the coherent gaps occur at least at two twin boundaries and the angles are different (figure 4). The dashed lines in figure 4 indicate the presence of stacking faults along with twin boundaries. [9]
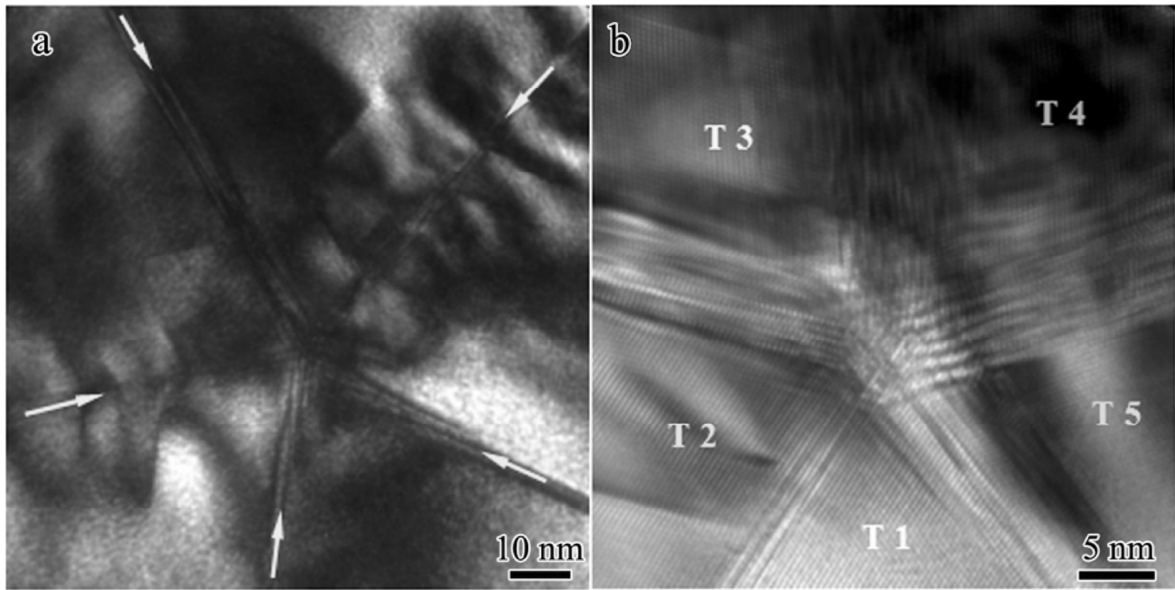

Figure 3. (a) Low-magnification TEM image of the Ag NW's cross-section showing five juxtaposed crystals. (b) High-resolution TEM image of the center area of an Ag nanorod cross-section, where five distinctive {111} twin boundaries are shown. The subcrystals are labeled as T1, T2, T3, T4, and T5, respectively. [9]
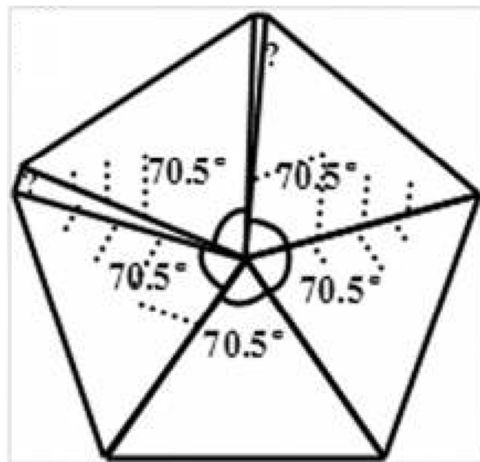

Figure 4. Pentatetrahedral twin model for an Ag nanorod. [9]

2.3.3 Mechanical properties of silver nanowires

Available studies on mechanical characterization of pentagonal Ag NWs report Young's moduli in the range of 63 to 176 GPa [1, 10, 11], while bulk Young's modulus is (83 GPa) [19]. Zhu et al. attributed the elevated values of the Young's modulus to the fivefold twin microstructure of the NW and the surface effect [1]. This structure makes the NW more brittle, but also less ductile. Increased brittleness compared to bulk Ag was also observed by Leach et al. [25] when performing tensile test on pentagonal NWs in molecular dynamics. Here also, the higher Young's modulus and lower plasticity was attributed to fivefold twinned boundaries. The {111} twin boundaries restrict the movement of partial dislocations, which limits the strain of the NW before failure.

2.4 Techniques for measurements of mechanical properties of NWs

Due to the small dimensions mechanical characterization of nanostructures is challenging task and that requires the use of advanced techniques. Commonly measurements are performed either with atomic force microscope (AFM) or inside scanning / transmission electron microscopes (SEM or TEM) using fine positioners.

In this part a brief overview of existing techniques for mechanical characterization of NWs is given.

2.4.1 AFM based methods

2.4.1.1 AFM

AFM is a scanning microscope that can produce very high-resolution, 3-D images of sample surface. The AFM measures ultra small forces (less than 1 nN) present between the AFM tip surface and a sample surface. These small forces are measured by measuring the motion of a very flexible cantilever beam with an ultra small mass. The sample can be scanned by means of a piezoactuator, the cantilever deflection may be measured in different ways in order to reproduce the sample topography. AFMs are capable of investigating the surfaces of both conductors and insulators on an atomic scale if suitable techniques for measuring the cantilever motion are used. [26, 27]
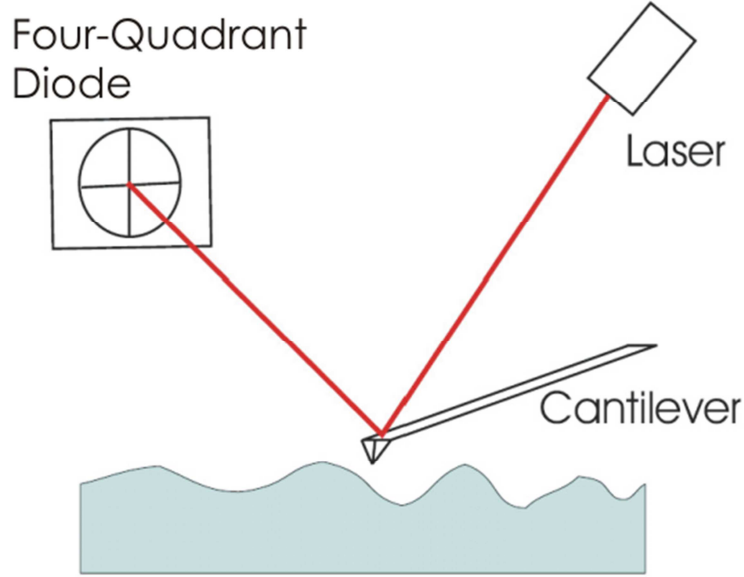
Figure 5. Working principle of AFM. [28]

2.4.1.2 Three point bending test with an AFM

In this method, the mechanical properties of the NW are measured by performing three-point bending tests on NWs suspended, for example, over holes or trenches inside an AFM. The AFM cantilever tip is used to apply small force at the middle point along suspended part of NW (figure 6). Three point bending test has been applied to Ag NWs [10, 11]. In the work of Jing et al. [10] the Ag NWs were lying over a hole etched in a silicon wafer. The AFM measurements were performed in vacuum to avoid the presence of thin layer of water and other contaminants affecting the measurement. Before measurement with AFM, SEM images were obtained to determine the positions of the suspended NWs over the holes. Low magnification AFM images of the sample were taken in order to select a suitable NW. Then a high magnification AFM images was carefully scanned. The diameter of selected NW was measured from the SEM image and the suspended length was measured from the AFM image. Then the measurement was performed. No permanent deformation of the NWs was detected. The adhesion between the NW and the silicon substrate was found to satisfy the assumption that both ends of the NWs are clamped as the NW ends are found to remain in place even after the test is conducted. The Young's modulus of the NW was found by using Timoshenko's beam theory for three-point bending, where Young's modulus E is defined as:

$$E = L^3 k_s / (3\pi D^4) \qquad (1)$$

where L is the length of the suspended part of the NW, D is the diameter and k_s is the stiffness of the NW.

Obtained Young's moduli ranged from 60 to 160 GPa. Also the size effect was observed, i.e. the Young's modulus increased with the decrease of NW diameter. For NWs with diameters greater than 100 nm, the measured values approached a constant value, which was lower than that of the bulk Ag. However, NWs with diameters around 20 nm had modulus values approximately two or three times that of the bulk. [10]
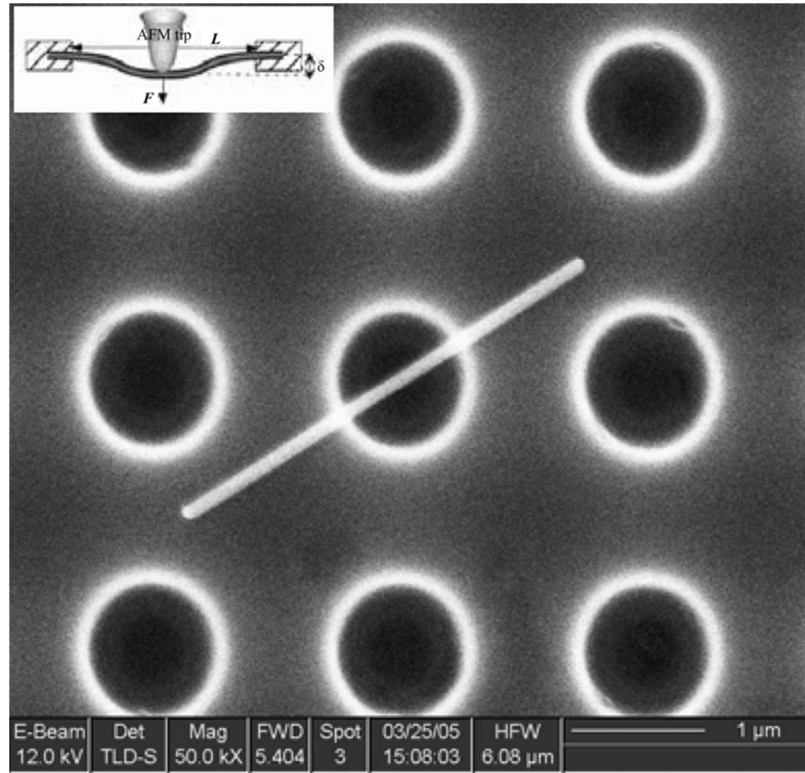

Figure 6. SEM image of a suspended NW. Inset shows a schematic diagram of a NW with midpoint deflected by an AFM tip. [10]

In the work of Wu et al. [11] the Ag NWs were suspended over a trench. Well-defined trench patterns were fabricated on a substrate that was coated with a 10-20 nm TiN film. Suitable NWs crossing the trench patterns were located by SEM in a dual-beam (electron/focused ion beam) system and then double-clamped at the trench edges by electron-beam-induced deposition (EBID) of Pt lines. The measurements were performed with AFM at ambient conditions. Here, the bending test was lateral. The AFM tip was positioned into the trench, above the trench base, and a lateral force was applied to the NW. Bending measurements were either a single-shot experiment (in which the tip engaged the wire, elastically and then plastically deformed it, and finally broke the wire in a single manipulation) or in a series of loading-unloading cycles (in which the wire was increasingly loaded and unloaded in a series of manipulations so that progressive elastic and then plastic deformation occurred, followed by wire failure). According to authors, fracture of NW was brittle, which is unusual for ductile material like Ag. However, no

analysis of fractured area and residual deformation was made to clarify exact mechanism of fracture. The average Young's modulus value of measured NWs, with diameters from 22 to 35 nm, was 102 ± 23 GPa.
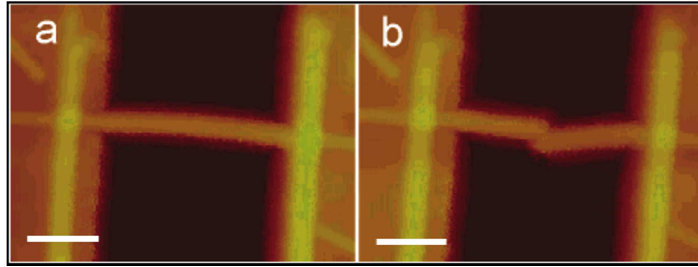

Figure 7. AFM images of an Ag NW (a) before bending and (b) after brittle failure. Both scale bars are 250 nm. [11]

2.4.1.3 Nanoindentation

Another AFM-based method for measuring mechanical properties of NWs is nanoindentation. Here AFM tip is used to make the indent on the NW. This method was also used to study Ag NWs [13]. Ag NWs were deposited on an oxidized silicon wafer and measurements were performed with AFM at room temperature and ambient conditions. AFM topography images were taken before and after the nanoindentation test with the same tip in the tapping mode. The normal force was calibrated by recording the deflection of the cantilever as a function of the scanner displacement while in contact with the substrate. AFM images were used to locate the NW and position the tip over the middle of the NW to gather the force-depth curve. The loading force-depth curve was converted to an indentation stress-strain. The indentation stress was obtained by dividing each force value by the corresponding instantaneous contact area. The contact area was estimated by considering a perfectly spherical tip indenting a pentagonal NW that had ideal plastic deformation behavior. At a particular indent depth, the contact area was defined as the projected area of the section of the tip that penetrated the pentagonal NW. The indentation strain was defined as the ratio between the instantaneous contact radius and the tip radius. The contact radius was the radius of the equivalent circle of contact delimiting the contact area.

Lucas et al. [13] performed nanoindentation test on a pentagonal Ag NW (D = 40 nm) and obtained maximum stress of 2 GPa.
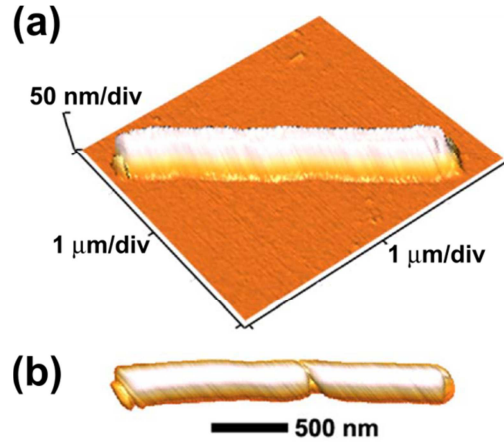
15

Figure 8. AFM images of a Ag NW (a) before and (b) after the nanoindentation (top view). [13]

2.4.1.4 Limitations of AFM-based methods

A major disadvantage of AFM-based measurements is that there is no visual feedback during the experiment, i.e. imaging and probing cannot be done simultaneously. Moreover, due to the fact that many AFM systems don't have vacuum capability, experiments are done in ambient conditions, which means presence of thin layer of water and other contaminants affecting the measurement.

2.4.2 Measurements inside electron microscopes

More advanced measurements are performed inside electron microscopes to provide vacuum environment and real-time visual feedback of the experiment.

2.4.2.1 Tensile test in SEM

One of the methods for measuring the mechanical properties of NWs is tensile test inside SEM. Method was applied to Ag NWs by Zhu et al. [1] In his work NW was clamped on the nanomanipulator tip at one end and the AFM cantilever at another using EBID of carbonaceous materials in the SEM, figure 9. The nanomanipulator was used to apply force to the NW and it was measured by the AFM cantilever. The drop-cast method used to prepare the NW samples ensures the NWs are perpendicular to the electron beam; thus, no out-of-plane rotation is coupled to the tension, and the strain measurement should be accurate. A small in-plane rotation might occur during the tension process as a result of the deflection of the AFM cantilever. An AFM cantilever with relatively large stiffness was selected to ensure such in-plane rotation is negligible. The NW was then loaded in tension until failure to investigate the full spectrum of

mechanical properties, including elastic, plastic, and failure properties. A series of SEM images were taken during the tension tests. Both force and elongation were measured from the images and converted to stress and strain, respectively. Force was obtained by multiplying the force sensor's (AFM cantilever's) displacement by its calibrated stiffness.

Obtained results showed presence of size effect. The Young's modulus increased with the decreasing diameter. Highest Young's modulus was 176 GPa, for NW with diameter of 34 nm. NWs with diameters larger than 80 nm appeared to have slightly lower Young's moduli than the bulk value. [1]

In contrast to AFM-based experiments, real-time visual feedback during the experiment allows to observe the elongation, the neck formation and the ultimate failure of the NW. The accuracy of the method relies on determination of NW elongation and cantilever deflection, which, in turn, depend on SEM resolution.
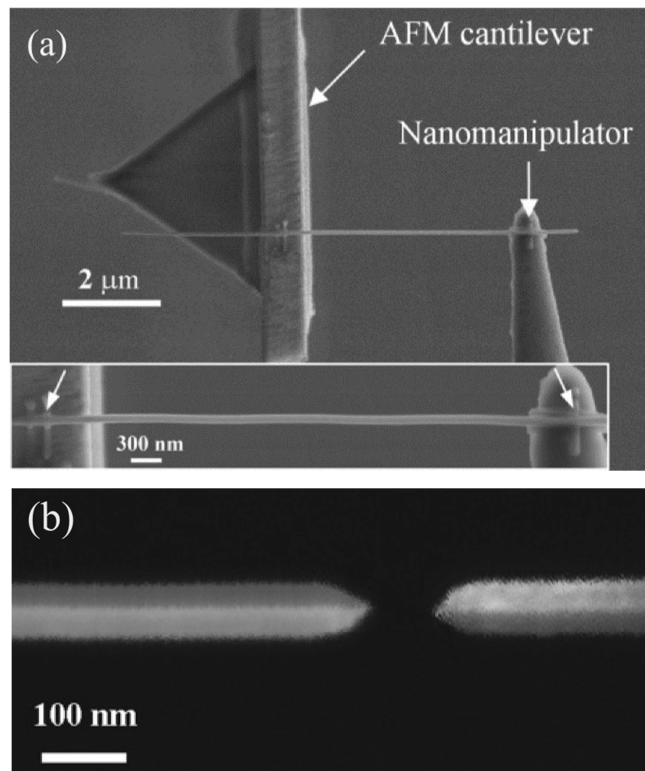

Figure 9. (a) SEM image showing the tensile test of a single NW. High-resolution SEM image of the NW for strain measurement is shown in the inset. The clamps by EBID are indicated by two arrows. (b) SEM image showing the fracture surfaces of the Ag NW. [1]

2.4.2.2 Mechanical resonance method

Another method for determining the Young's modulus is mechanical resonance method. Mechanical resonance in a NW can be induced when the frequency of the applied periodic force

approaches the NW's resonance frequency. According to Euler–Bernoulli beam theory, the nth mode frequency, f_n, of a cantilevered uniform beam is:

$$f_n = \frac{\beta_n^2}{2\pi}\sqrt{\frac{EI}{mL^4}} \qquad (2)$$

where E is the Young's modulus of the beam, I is the cross-section moment of inertia, m is the mass per unit length and L is the beam length. The β_n term is the eigenvalue from the characteristic equation: $\cos(\beta_n)\cosh(\beta_n) + 1 = 0$; β_1=1.875 corresponds to the first resonance mode for any cantilevered beam. [29]

Mechanical resonance method has been used to study the mechanical properties of various NWs, nanotubes, and nanobelts [29], however it has never been applied to Ag NWs.

Smith et al. [30] deposited germanium NWs onto a TEM grid (copper substrate) that was then mounted on a SEM stage and placed in a dual beam SEM/FIB system equipped with a nanomanipulator. Suitable NWs for the experiment were identified in SEM mode. To prevent slippage of the NW during oscillation Pt was deposited by EBID at the junction between the copper substrate and the NW. Mechanical oscillations of the NWs were excited by applying an AC voltage between two nanomanipulator's tungsten nanoprobes attached to a frequency response analyzer. One probe was contacted to the copper grid and the second was held within a micrometer of the NW tip. Measurements were carried out by applying a sinusoidal voltage sweep. The AC frequency was scanned until the NW was observed to oscillate. Many images of the oscillating NW were obtained by SEM. The vibrational amplitude was determined visually using image processing software. The cantilever length was determined from SEM images and the NW diameters were determined by TEM.
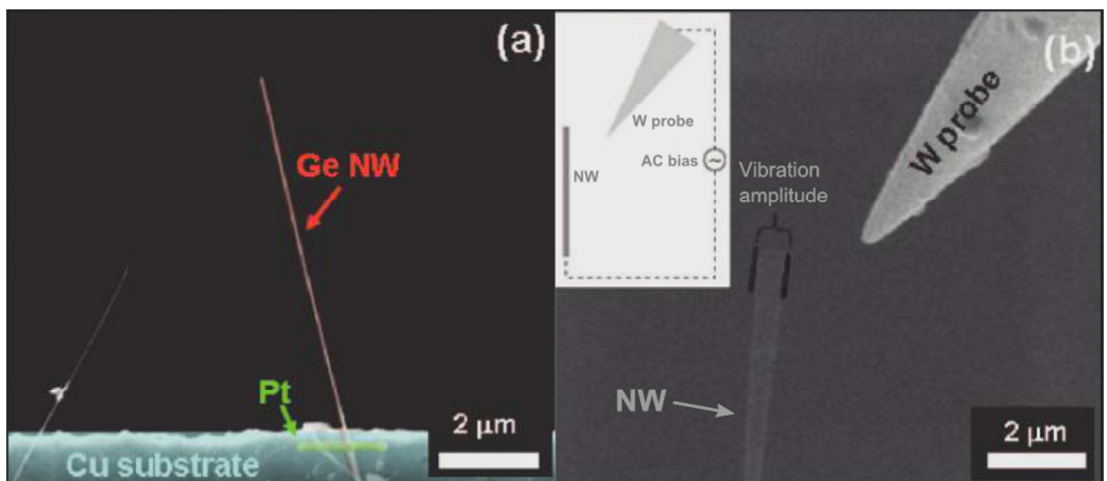

Figure 10. (a) SEM image of a Ge NW cantilever: the NW is glued to the Cu substrate with Pt deposited by electron beam-induced deposition in the SEM/FIB tool. (b) SEM image of an Ge NW vibrating in response to a sinusoidal potential applied by the nearby tungsten probe. (Inset) Device schematic. [30]

Another possible way to excite NW into oscillation is by applying mechanically induced periodic force. This method was used by Ding et al. [29] to determine the Young's modulus of boron NWs. They also performed the measurements inside a SEM. A NW was clamped to the tip of the AFM cantilever using EBID. The AFM cantilever was mounted on the end of a piezoelectric multi-layer bender that was mounted to the *X–Y* linear motion stage. By applying an AC voltage to the piezoelectric bender to induce mechanical oscillation, they caused the attached NW to mechanically oscillate.
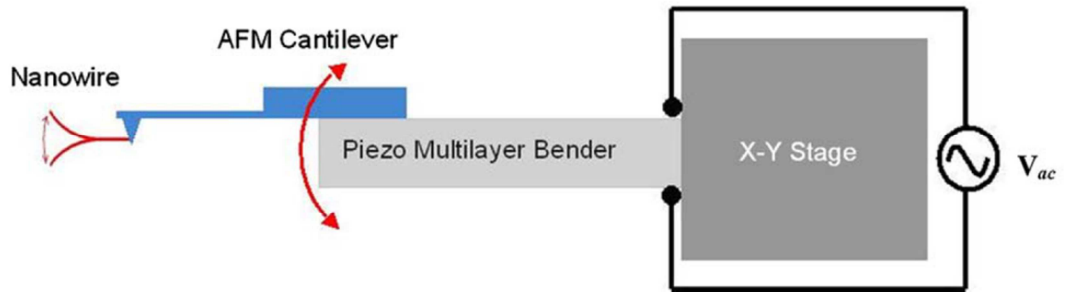

Figure 11. Experimental setup for mechanical excitation of a cantilevered NW. [29]

In contrast to other mechanical characterization techniques, mechanical resonance method benefits from being non-destructive. However, resonance frequencies of NWs are usually very high, in the range of several MHz, with a sharp resonance peak, which makes founding of resonance technically difficult.

Although some of listed methods were applied for mechanical characterization of Ag NWs, important case of pure bending was not realized in reported test conditions. Pure bending, however, is highly important from applicative point of view, e.g. in flexible transparent electrodes [4], nanoswitches [5], and resonators [6].

3. Experimental part

In this part the experimental details of mechanical characterization of Ag NWs with cantilevered beam bending technique performed inside SEM are described. Measurements also include fatigue bending tests. Young's modulus and yield strength of Ag NWs extracted using the elastic beam theory. Finally, results of bending tests are discussed and analyzed.

3.1 Materials

Ag NWs were purchased from *Blue Nano* and had diameter in the range from tens to few hundred nm with average diameter of 120 nm. High-resolution SEM (Helios NanoLab, FEI) images revealed straight and uniform NWs with well-pronounced pentagonal cross-section (figure 12). The silicon calibration grating (TGX series, Mikromasch) was used as substrate. TGX grating comprised of 1 µm deep square holes with 3 µm pitch having sharp undercut edges formed by the (110) crystallographic planes of silicon. Ag NWs were deposited on grating from ethanol solution so that some NWs were partly suspended over the trenches.
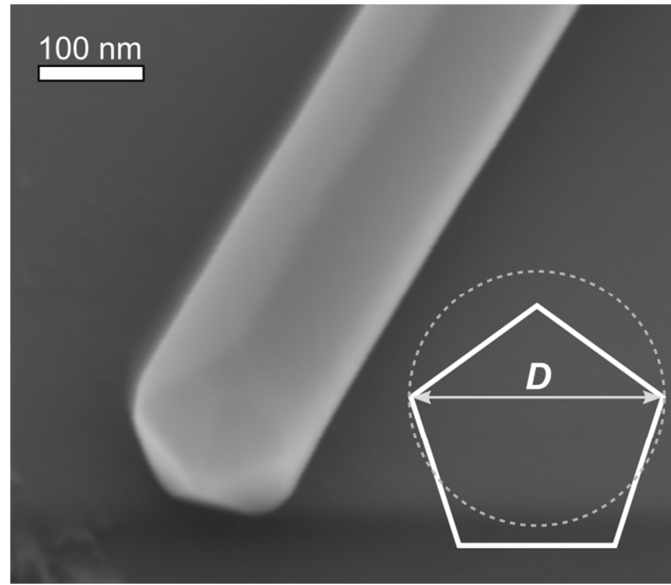

Figure 12. SEM micrograph of one of the Ag NWs used in bending tests and schematic of pentagonal cross section with apparent diameter D. Circular cross-section of the same D is given for representative purpose.

3.2 Experimental set-up

Recently developed *insitu* nanomanipulation and measurement set-up [31] was used in the experiment. System was comprised of 3D nanomanipulator (SLC-1720-S, SmarAct) equipped with self-made force sensor and installed inside SEM (Vega-II SBU, TESCAN; typical chamber vacuum 3×10^{-4} mbar). Force sensor was made by gluing the AFM cantilever with a

sharp tip (Nanosensor ATEC-CONT cantilevers C=0.2 N/m) to one prong of a commercially available quartz tuning fork (QTF). The tip of ATEC-CONT cantilevers is tilted about 15 degrees relative to the cantilever, providing tip visibility from the top. In experiments QTF is driven electrically on its resonance frequency in self-oscillation mode. Oscillation parameters of such system strongly depend on the forces acting on the tip, which enables to measure the forces involved in manipulations. The signal from the QTF was amplified by lock-in amplifier (SR830, Stanford Research Systems) and recorded through the ADC-DAC card (NI PCI-6036E, National Instruments). The typical values of the driving voltage were 20-50 mV and corresponding tip oscillation amplitude in order of 100 nm. In experiments, tip oscillated parallel to the sample surface (shear mode) and normal to NWs.

The force sensitivity of the sensor was calibrated on pre-calibrated AFM cantilevers (FCL, AppNano and CSG11 C=0.03-0.1 N/m, NT-MDT) similar to the procedures described in [32, 33].

The tip was electrically connected to the QTF electrode to exclude charging effects. To make the QTF response faster, the Q-factor was reasonably decreased by putting a small drop of epoxy resin (Ecobond 286, Emerson & Cuming) onto the opposite prong of the QTF.

3.3 Bending test

Advanced cantilevered beam bending scheme was employed to measure Young's modulus, yield strength and fatigue of Ag NWs. Measurements consisted in visually controllable in-plane bending of half-suspended NW by AFM tip inside SEM with simultaneous force registration. No special procedures were needed for fastening the NWs to the substrate, due to the static friction between the NW and the substrate that was high enough to keep the adhered part of the NW in place during the bending.

After the bending tests all NWs were characterized inside high resolution SEM to obtain precise data on diameters and analyze the deformed area of NW.

Compared to previously mentioned AFM-based methods, bending test inside SEM gives immediate visual feedback. Also results from bending test are easier to interpret and conclusions are more reliable than in three-point bending test, where both bending and tensile deformations are involved.
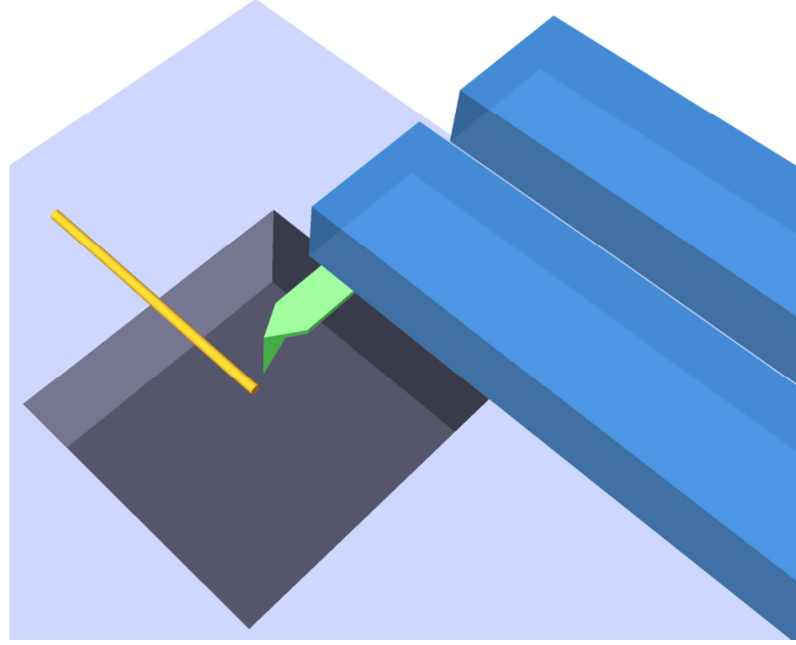
Figure 13. Schematics of the cantilevered beam bending test scheme used in present study: half-suspended Ag NW and self-made force sensor (AFM tip glued to one prong of QTF).

3.4 Theoretical analysis of experimental data

Numerical analysis of the bending test was based on the elastic beam theory [34]. The equation of the equilibrium for a bent elastic beam with Young's modulus E and area moment of inertia I loaded by a point force f at its end can be written as [35]:

$$E \cdot I \cdot \frac{d^2\theta}{dl^2} + f \cdot cos\theta = 0 \qquad (3),$$

where θ is the angle between the tangent of the bent NW profile projected on an initial NW profile as a function along the NW axis.

The area moment of inertia for pentagonal cross-section can be written as following:

$$I_{pent} = \frac{1}{96}\frac{(3-\sqrt{5})}{(3+\sqrt{5})}\sqrt{256 + 118\sqrt{5}}D^4 \quad (4),$$

where D is the width of NW, as it is seen from top inside SEM and can be understood from the figure 12. The equation (3) can be solved numerically with the boundary conditions:

$$\theta|_{l=0} = 0 \qquad (5a)$$

$$\frac{d\theta}{dl}\Big|_{l=L} = 0 \qquad (5b)$$

where l is the natural axis of the NW and L is the length of the suspended part of the NW. Equation (5a) implies that the NW is fixed along its axis in the adhered part, and equation (5b) is dictated by the absence of momentum at the end of the NW.

This model enables to find out the flexural rigidity of the NW, which is a product of the Young's modulus E and area moment of inertia I. Young's modulus is intrinsic property of

material, and area moment of inertia is determined by the cross-sectional geometry of NW. Ag NW was modeled as prismatic beam with pentagonal cross-section. Force-displacement curve within the approximation of pure in-plane bending of elastic beam of a given EI was calculated. The experimental and modeled force-displacement curves were fitted for the determination of E as unknown parameter. The yield point was identified as the point where curves divergence.

SEM images of the NW profiles were numerically fitted to the bending profile given by $\theta(l)$ according to equation (3) and consequently, the value of Young's modulus was extracted. A specific script in *Wolfram Mathematica* was made for this purpose.

The maximal tensile stress σ_{max} and tensile strain ε_{max} in elastically deformed NW occurring on the outermost side of NW can be expressed as a function of local NW curvature $\kappa=d\theta/dl$ from the bending profile as well:

$$\sigma_{max} = ED\kappa/2 \qquad (6a)$$

$$\varepsilon_{max} = D\kappa/2 \qquad (6b) \qquad (4a)$$

At the point of the transition from elastic to plastic regimes, those quantities will have meaning of yield strength and yield strain.
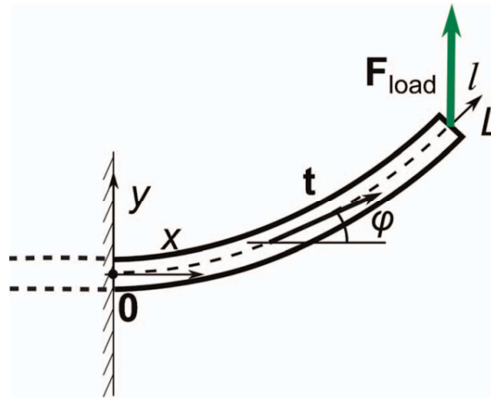
Figure 14. Schematics of NW fixed at one end and loaded at the other end by concentrated force F_{load} [36].

3.5 Results and discussion

3.5.1 Bending tests

Measurements were performed on 20 NWs with diameters ranging from 76 nm to 211 nm. Typically two regions were clearly distinguished on bending curves as shown on figure 15. In initial region (*a-b*) NW bends elastically. It was also confirmed separately on several NWs

that in the linear region removal of external force will cause the NW to return to the undeformed state. Then the slope of force curve changes, which indicates the onset of plastic yield. The following region (*b-c*) corresponds to plastic deformation of the wire. At the region *c-d* the tip is retracted and the force drops to zero. The same NW was then deformed more to find the critical deformation before fracture. However, as seen from figure 15 (f) even strongly bent NW has no signs of fracture, and deformation seems to be purely plastic, indicating significant difference of Ag NW behavior in pure bending conditions in comparison to "super elastic behavior followed by unexpected brittle failure" [1] and brittle fracture [11] reported in three point bending and tensile tests respectively.
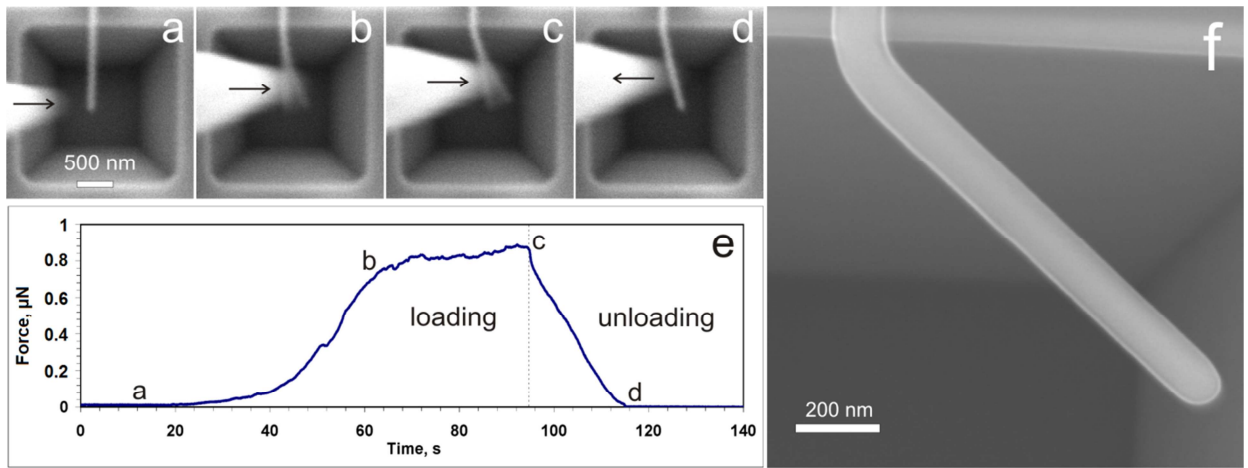

Figure 15. Bending test of Ag NW. Selected frames from video of experiment (a-d), corresponding force curve vs time (e), and high-resolution SEM image of plastically bent NW after the experiment (f).

Nevertheless about one third of NWs did break during bending (figure 16).In this case three regions on the force curve can be distinguished. Incident elastic bending (*a-b*) is followed by steep drop in force (point *b*), which may correspond to partial destruction of NW and crack formation. Region *b-c* may indicate crack stabilization and plastic deformation during further bending. Finally NW breaks (point *c*). Event of breaking is accurately detected both from the video of the experiment and from the abrupt drop of the force close to zero after the point *c*. Subsequent observation in high-resolution SEM revealed rather brittle fracture of broken NWs without noticeable residual deformation (figure 16). Such behavior is not what one would expect from plastic material like Ag, however, now it conforms to brittle fracture reported in tensile and three point bending tests [1, 11]. On the other hand, broken end still remained partly attached to the rest of NW in all the cases of fracture, which is not typical for purely brittle fracture. Moreover, very small, but nonzero force is still detectable after fracture, which may indicate the presence of a small neck connecting two parts of the NW. Thus, fracture mechanism seems to be

more complex possessing attributes of both plastic and brittle fracture. Such duality may be related to pentagonal structure of Ag NWs, which leads to the presence of intrinsic elastic strain due to peculiarities of their fivefold twinned structure [9, 24]. The intrinsic strain possessing elastic energy can facilitate the plastic flow processes. On the other side, the twin boundaries might decrease the mobility of defects. Therefore detailed analysis and simulations of bending deformation is required.
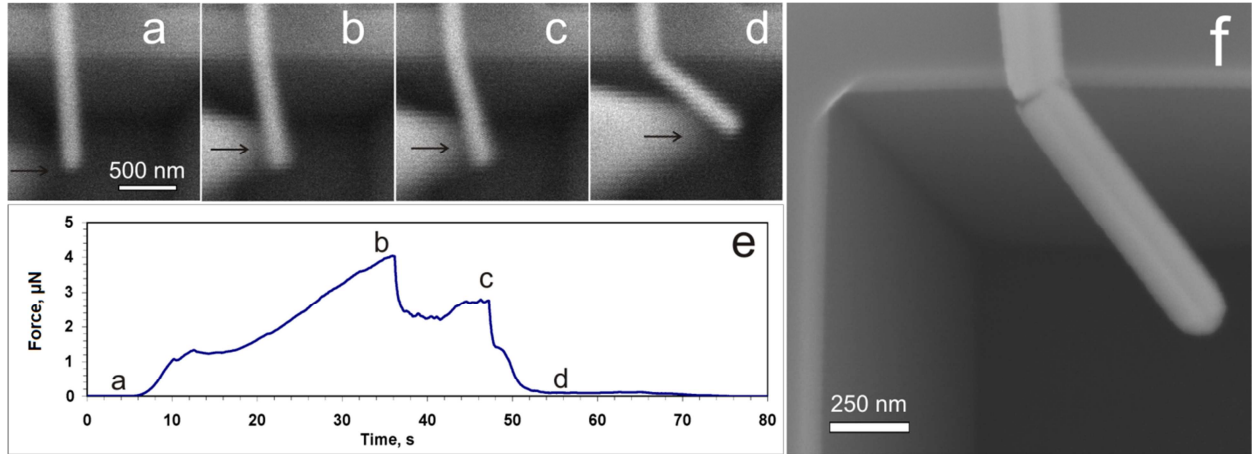

Figure 16. Bending test of Ag NW. Selected frames from video of experiment (a-d), corresponding force curve vs time (e), and high-resolution SEM image of broken NW after the experiment (f).

Degree of deformation Ag NWs withstood prior yield and fracture was relatively high. Median curvature and strain in elastic regime were 0.8 ± 0.3 μm^{-1} and $9.3\% \pm 3.5\%$ respectively.

3.5.2 Fatigue test

Oscillation frequency of the tip in experiments was approximately 30 kHz. This allowed us to perform the fatigue tests of NWs and evaluate influence of tip oscillations on NWs deformation during bending test. The tip was brought into contact with NW and oscillation amplitude was increased to value close to maximal deformation prior plastic yield. The tip-NW system was left to oscillate for several minutes producing several millions of bending cycles. No signs of fracture or plastic deformation, as well as changes in a force sensor signal, were observed indicating high fatigue resistance of Ag NWs. However, influence of the tip oscillation on NWs deformation during bending tests cannot be excluded completely. For example, mechanical excitation from the QTF can lead to heat dissipation and local elevation of the temperature. In this case increased mobility of defects can promote the plastic regime of deformation. Therefore problems like fatigue, as well as mechanism of deformation and fracture, need to be addressed in future researches and studied systematically. Nevertheless, it can be

concluded that Ag NWs can be bent elastically multiple times to significant curvatures without fracture and therefore are suitable for most NEMS applications.

3.5.3 Young's modulus and yield strength

For numerical analysis of the experimental data the force curves and NW profiles from the SEM images were fitted to the curve given by the equation of equilibrium for a bent elastic beam [36]. Fitting of experimental and modeled force-displacement curves is shown on figure 17. Point of divergence of two curves corresponds to the onset of plastic yield.
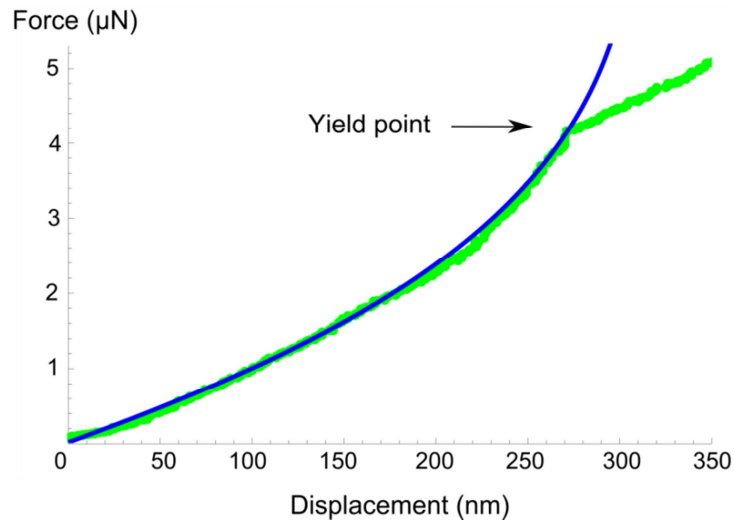

Figure 17. Fit of experimental and theoretical force-distance curves, which gives Young's modulus and yield strength of 113 GPa and 10 GPa respectively.

Measured Young's moduli ranged from 39 GPa to 150 GPa with median of 90 GPa, which is only slightly higher than bulk value 83 GPa [19] of Ag. Yield strength values are scattered without pronounced peak from 1 GPa to 10 GPa with median average of 4.8 GPa, which is two orders of magnitude higher than that of bulk Ag (which is around 50 MPa) [19]. The large scattering of results can be attributed to random distribution of defects in individual NWs.

No correlations of measured properties with NW diameter was observed, which is in accordance to expectation for considered diameters. In other works it was shown that Young's modulus approaches a constant value for Ag NWs thicker than 70 nm [10, 37].
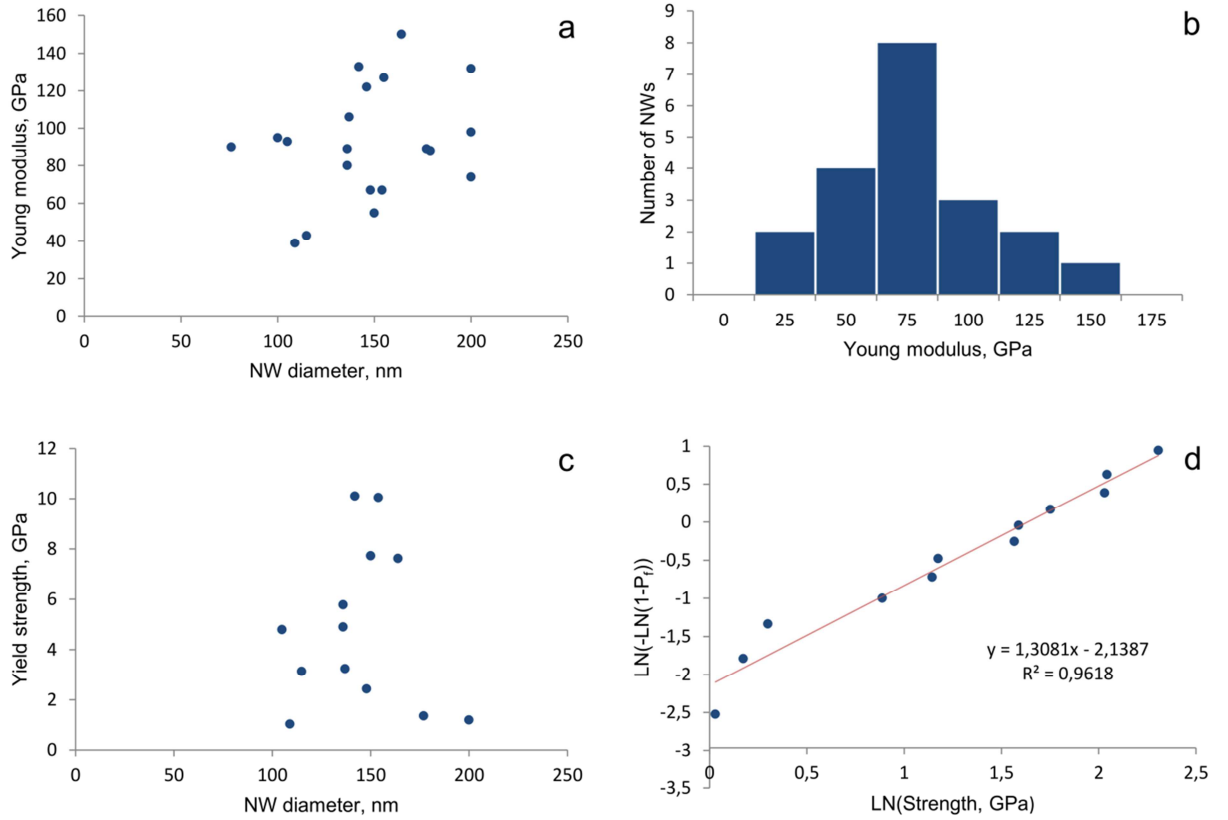
Figure 18. Young's modulus versus diameter (a), distribution of Young's moduli (b) for set of 20 NWs, yield strength versus diameter (c), and plot of Weibull statistics (d).

3.5.4 Weibull statistics

Common way to analyze and represent the distribution of material's strength is Weibull statistics [38, 39]. The probability of failure or deformation for a specimen at an applied stress σ_f is given as:

$$P_f = 1 - \exp[-(\frac{\sigma_f}{\sigma_{0A}})^m] \qquad (7)$$

where σ_o is the characteristic strength (i.e., the stress at which 63% of the specimens have failed or deformed plastically), and m is the Weibull modulus (also called the shape parameter). The Weibull modulus is a dimensionless parameter of the Weibull distribution used to describe variability in the measured strength. Higher m values correspond to a steeper Weibull plot and indicate a lower dispersion of fracture stresses. In this experiment the obtained Weibull modulus was 1.31, which is much lower than in Zhu et al. [1]. However, the characteristic strength of 5.1 GPa obtained by us, was higher than Zhu et al. reported. This can be due to different measuring method or difference in NW quality.

3.5.5 Sources of error

Measurements at the nanoscale are much more complicated than macroscopic characterization of materials, and there is always number of things to be considered and discussed.

In experiments the tip is not strictly perpendicular to the NW, but under slight obtuse angle to provide tip visibility from the top. It may cause minor slippage of NW along the tip in vertical direction. Considerable slippage would be clearly seen from the SEM experiment video, however small vertical displacements still could take place and contribute to data scattering.

One of the most critical parameter in determination of Young's modulus and yield strength in described method is diameter of NW. According to the equation (3), error in diameter will cause approx. four times higher error in Young's modulus. For this reason diameters of all NWs used in experiment was measured in high-resolution SEM.

Cross-sectional geometry of NWs within frameworks of elastic beam theory can also be a source of error. This will be closely discussed in the following section.

3.5.5.1 Young's modulus and yield strength dependence on NWs cross-sectional geometry

Although pentagonal symmetry is typical for Ag nanostructures [9, 21, 22], it is common that researchers chose circular geometry for their calculations [10, 11, 12]. Indeed, such assumption can be partly justified since in some cases the cross-section of Ag NWs can be considerably rounded [11]. Nevertheless, facets are still easily distinguishing, which leads to conclusion that the real geometry can lie somewhere between pentagon and circle.

Area moments of inertia for pentagonal I_{pent} and circular cross-section I_{circ} [40]:

$$I_{pent} = \frac{1}{96} \frac{(3-\sqrt{5})}{(3+\sqrt{5})} \sqrt{265 + 118\sqrt{5}} D^4 \quad (8)$$

$$I_{circ} = \frac{\pi}{64} D^4 \qquad\qquad (9)$$

where D is an apparent diameter and can be understood from the inset on figure 12. Now if to compare Young's moduli of the beams with the same D, but different cross-sections, E_{pent}/E_{circ}=1.405 is obtained. Thus, circular assumption gives underestimated results in bending tests of pentagonal NWs. This can be a possible reason of low Young's moduli (below bulk value) obtained by Jing et al. for diameters greater than 90 nm [10].

In addition to rounding, distortions of pentagon are also reported in literature [24]. Facets, as well as the angles between facets, are not always equal. As an example, possible influence of unaccounted pentagon geometry distortion on Young's modulus was estimated for the case of

pentagon compressed to different extent in direction normal to apparent diameter D. For compression factor varying from 0.8 to 1.2 Young's moduli of particular NW ranging from 115 to 75 GPa was obtained. It is necessary to note, that pentagon distortions cannot be easily detected from the top view of the SEM image if distorted facet hidden under a NW. Therefore, unaccounted deviations from regular pentagonal geometry may significantly contribute to data scattering.

4. Summary and conclusion

Silver nanowires (Ag NWs) have many attractive properties and promising applications. However, mechanical properties of single Ag NWs are poorly studied. Only few works on tensile and three-point bending tests of Ag NWs are available in literature.

In this thesis mechanical properties of Ag NWs were characterized using cantilevered beam bending technique inside scanning electron microscope (SEM). In this method pure bending conditions are realized, which are highly important from applicative point of view. According to literature, this method has never been used to study mechanical properties of Ag NWs before.

Chemically synthesized Ag NWs were deposited from ethanol solution on silicon grating containing square holes so that some NWs were partly suspended over the trenches. Measurements consisted in bending of cantilevered NWs with AFM tip glued to self-made force sensor. Bending tests were performed on twenty Ag NWs with diameters ranging from 76 nm to 211 nm.

Relatively high degree of elasticity followed by either plastic deformation or fracture was observed in bending experiments. Experimental data was numerically fitted into the model based on elastic beam theory and values of Young's modulus and yield strength were extracted. Median Young's modulus was found to be 90 GPa. It is just a slightly higher than 83 GPa for a bulk Ag and is in accordance with expectations for considered diameters: significant increase of elastic modulus for nanostructures is typically observed for sizes much below 100 nm. Measured average yield strength was 4.8 GPa, which is two orders of magnitude higher than that of bulk Ag (around 50 MPa). Measurements results were highly scattered, which was attributed to random distribution of defects in individual NWs. In addition, fatigue tests with several millions of cycles were performed and it was shown that Ag NWs have high fatigue resistance and can be bent elastically multiple times to significant curvatures without failure. Moreover, it was demonstrated that circular assumption typically made by other authors when calculating mechanical properties of pentagonal Ag NWs can lead to significant errors in results. Therefore pentagonal cross-section was used in this thesis.

From the results of present study it can be concluded that mechanical properties of Ag NWs are suitable for NEMS applications like nanoswitches, nanorelays, and nanoresonators.

Author's contribution

The experiments presented in the thesis were made in a team work. However, author participated in the study from the very beginning to the end and contributed to all its main stages. In particular:

- Author performed preparation of substrates and characterization of Ag nanowires.
- Author prepared several QTF-based force sensors.
- Author participated in / performed individually Young modulus and yield strength measurements of Ag nanowires inside scanning electron microscope.
- Author participated in data analysis and performed important calculations.

5. Summary in Estonian

Hõbe-nanotraatide mehaaniliste omaduste uurimine

Magnus Mets

Kokkuvõte

Hõbe-nanotraatidel on mitmeid tähelepanu väärseid omadusi nagu väga hea elektri- ja soojusjuhtivus. Sellest tulenevalt on neil ka paljulubavaid rakendusi, näiteks läbipaistvad painduvad elektroodid ekraanides, nanolülitid ja nanoresonaatorid. Sellest hoolimata on üksikute hõbe-nanotraatide omadusi vähe uuritud. Vaid mõned tööd on publitseeritud hõbe-nanotraatide tõmbe- ja kolme-punkti-paindekatse teemal.

Käesolevas bakalaureusetöö raames karakteriseeriti hõbe-nanotraatide mehaanilisi omadusi kasutades konsooli painde tehnikat skaneerivas elektron mikroskoobis. Antud meetodiga saavutatakse puhta painde tingimused, mis on väga tähtsad rakenduslikku aspekti silmas pidades. Toetudes kirjanduse analüüsile saab öelda, et antud meetodit ei ole varem kasutatud hõbe-nanotraatide mehaaniliste omaduste uurimiseks.

Katses kasutatud hõbe-nanotraadid olid keemiliselt sünteesitud. Etanooli lahuses olevad nanotraadid viidi räni alusele, milles olid ruudukujulised augud. Etanooli aurustudes asetsesid osad nanotraadid osaliselt aukude kohal. Mõõtmiste käigus painutati nanotraatide vabu otsi aatomjõu mikroskoobi teravikuga. Teravik oli liimitud isevalmistatud jõusensori külge, milleks oli kalibreeritud helihargi tüüpi kvartsresonaator. Paindekatseid korraldati kahekümne hõbe-nanotraadiga, diameetritega 76 nm kuni 211 nm.

Paindekatses täheldati nanotraatide suhteliselt suurt elastsust. Elastse deformatsiooni piirkonnale järgnes nanotraadi plastne deformatsioon või purunemine. Sobitades eksperimentaalseid andmeid elastsete varraste teoorial põhineva mudeliga, leiti nanotraatide Youngi mooduli ja voolavuspiiri väärtused. Youngi mooduli mediaanväärtuseks oli 90 GPa. See on veidi kõrgem kui makroskoopilise hõbeda Youngi mooduli väärtus, milleks on 83 GPa. See tulemus oli ootuspärane arvestades nanotraatide diameetreid. Märkimisväärset Youngi mooduli tõusu on tüüpiliselt täheldatud nanostruktuuridel, milledel on diameeter tunduvalt alla 100 nm. Voolavuspiiri keskmine väärtus oli 4.8 GPa. See on kaks suurusjärku suurem makroskoopilise hõbeda voolavuspiirist, mis on umbes 50 MPa. Mõõtmistulemused olid märkimisväärselt

hajutatud ning see omistati defektide juhuslikule jaotusele individuaalsetes nanotraatides. Lisaks viidi läbi väsimuskatsed, kus nanotraadid läbisid mitu miljonit paindetsüklit. Näidati hõbe-nanotraatide suurt väsimustugevust ning et neid saab mitmeid kordi elastselt painutada suurte kõverusteni ilma neid murdmata. Samuti demonstreeriti, et ringikujulise ristlõike lähenduse kasutamine, mida osad autorid on teinud pentagonaalsete hõbe-nanotraatide mehaaniliste omaduste arvutamisel, võib põhjustada olulisi vigu tulemustes. Seetõttu kasutati antud bakalaureusetöös pentagonaalse ristlõike lähendust nanotraatide modelleerimisel.

Käesoleva bakalaureusetöö tulemuste põhjal saab järeldada, et hõbe-nanotraadid on sobilikud nanoelektromehaaniliste süsteemide rakendusteks nagu näiteks nanolülitid, nanoreleed ja nanoresonaatorid.

6. References

[1] Y. Zhu, "Size effects on elasticity, yielding, and fracture of silver nanowires: *In Situ* experiments", Phys. Rev. B 85, 045443 (2012).

[2] B. Wiley, "Synthesis of Silver Nanostructures with Controlled Shapes and Properties", Accounts Chem. Res. 40, 1067–1076 (2007).

[3] K. K. Caswell, "Seedless, Surfactantless Wet Chemical Synthesis of Silver Nanowires", Nano Lett. 3, 667–669 (2003).

[4] J.-Y. Lee, "Solution-Processed Metal Nanowire Mesh Transparent Electrodes", Nano Lett. 8, 689–692 (2008).

[5] O.Y. Loh, "Nanoelectromechanical contact switches", Nat. Nanotechnol. 7, 283–295 (2012).

[6] M. Li, "Bottom-up assembly of large-area nanowire resonator arrays", Nat. Nanotechnol. 3, 88–92 (2008).

[7] W. Wang, "Light Propagation in Curved Silver Nanowire Plasmonic Waveguides", Nano Lett. 11, 1603 (2011).

[8] H. S. Park, "Surface-Stress-Driven Lattice Contraction Effects on the Extinction Spectra of Ultrasmall Silver Nanowires", J. Phys. Chem. C 114, 8741–8748 (2010).

[9] H. Chen, "Transmission-Electron-Microscopy Study on Fivefold Twinned Silver Nanorods", J. Phys. Chem. B 108, 12038–12043 (2004).

[10] G. Y. Jing, "Surface effects on elastic properties of silver nanowires: Contact atomic-force microscopy", Phys. Rev. B 73, 235409 (2006).

[11] B. Wu, "Microstructure-Hardened Silver Nanowires", Nano Lett. 6, 468–472 (2006).

[12] Y. Ding, "The elastic module of Ag nanowires prepared from electrochemical deposition", J. Alloys Compd. 474, 223–225 (2009).

[13] M. Lucas, "Plastic deformation of pentagonal silver nanowires: Comparison between AFM nanoindentation and atomistic simulations", Phys. Rev. B 77, 245420 (2008).

[14] Z. L. Wang, "Mechanical and electrostatic properties of carbon nanotubes and nanowires", Mater. Sci. Eng. C 16 3–10 (2001).

[15] M. S. Dresselhaus, "Nanowires", in *Springer Handbook of Nanotechnology*, B. Bhushan, ed. (Springer, Berlin, 2010), pp. 119-168.

[16] Y. Xia, "One-Dimensional Nanostructures: Synthesis, Characterization, and Applications", Adv. Mater. 15, 353–389 (2003).

[17] S. K. Lee, "Gallium nitride nanowires with a metal initiated metal-organic chemical vapor deposition (MOCVD) approach", Phys. Status Solidi B 241, 2775–2778 (2004).

[18] T. Trentler, "Solution-Liquid-Solid Growth of Crystalline III-V Semiconductors: An Analogy to Vapor-Liquid-Solid Growth", Science 270, 1791–1794 (1995).

[19] D.R. Smith, "Low-Temperature Properties of Silver", J. Res. Nat. Inst. Stand. Technol. 100, 119–171 (1995).

[20] D. R. Lide, *CRC Handbook of Chemistry and Physics*, 88th 2007-2008 ed. (CRC Press, Boca Raton, Florida, 2007).

[21] J. Reyes–Gasga, "On the structure of nanorods and nanowires with pentagonal corss-section", J. Cryst. Growth 286, 162–172 (2006).

[22] Y. Gao, "Silver nanowires with five-fold symmetric cross-section", J. Cryst. Growth 276, 606–612 (2005).

[23] L. M. Dorogin, *Structural and tribological properties of zero- and one-dimensional nanocrystals*, PhD Thesis, University of Tartu (Tartu University Press, Tartu, 2012).

[24] V. G. Gryaznov, "Pentagonal Symmetry and Disclinations in Small Particles", Cryst. Res. Technol. 34, 1091–1119 (1999).

[25] A. M. Leach, "Deformation of Top-Down and Bottom-Up Silver Nanowires", Adv. Funct. Mater. 17, 43–53 (2007).

[26] B. Bhushan, "Scanning Probe Microscopy - Principle of Operation, Instrumentation, and Probes", in *Springer Handbook of Nanotechnology*, B. Bhushan, ed. (Springer, Berlin, 2010), pp. 573-618.

[27] B. Cappella, "Force-distance curves by atomic force microscopy", http://www.see.ed.ac.uk/~vkoutsos/Force-distance%20curves%20by%20atomic%20force%20microscopy.pdf

[28] Kirchhoff-Institute for Physics, "Atomic Force Microscopy (AFM)", http://www.kip.uni-heidelberg.de/AG_Pucci/Instrumentation/AFM/

[29] W. Ding, "Mechanics of crystalline boron nanowires", Compos. Sci. Technol. 66, 1112–1124 (2006).

[30] D. Smith, "Young's Modulus and Size-Dependent Mechanical Quality Factor of Nanoelectromechanical Germanium Nanowire Resonators", J. Phys. Chem. C 112, 10725–10729 (2008).

[31] S. Vlassov, "Real-time manipulation of gold nanoparticles inside a scanning electron microscope", Solid State Commun. 151, 688–692 (2011).

[32] S.C. Fain, "Measuring average tip-sample forces in intermittent-contact (tapping) force microscopy in air", Appl. Phys. Lett. 76, 930–932 (2000).

[33] C. Su, "Direct measurement of tapping force with a cantilever deflection force sensor", Ultramicroscopy 100, 233–239(2004).

[34] S. Timoshenko, J. Goodier, *Theory of Elasticity*, second ed., (McGraw–Hill Book Company, New York, 1951).

[35] L. Landau, E. Lifshitz, *Theory of Elasticity*, third ed., vol. 7, (Butterworth-Heinemann, Oxford, 1986).

[36] L. M. Dorogin, "Real-time manipulation of ZnO nanowires on a flat surface employed for tribological measurements: Experimental methods and modeling", Phys. Status Solidi B 250, 305–317 (2013).

[37] S. Cuenot, "Surface tension effect on the mechanical properties of nanomaterials measured by atomic force microscopy", Phys. Rev. B 69, 165410 (2004).

[38] C. Lu, "On the bending strength of ZnO nanowires", Phys. Lett. A372, 6113–6115 (2008).

[39] A. H. Barber, "Stochastic strength of nanotubes: An appraisal of available data", Compos. Sci. Technol. 65, 2380–2384 (2005).

[40] E.W. Weisstein, "Area Moment of Inertia." From MathWorld, A Wolfram Web Resource. http://mathworld.wolfram.com/AreaMomentofInertia.html.

Non-exclusive licence to reproduce thesis and make thesis public

I, Magnus Mets

(date of birth: 06.02.1991),

1. herewith grant the University of Tartu a free permit (non-exclusive licence) to:

1.1. reproduce, for the purpose of preservation and making available to the public, including for addition to the DSpace digital archives until expiry of the term of validity of the copyright, and

1.2. make available to the public via the web environment of the University of Tartu, including via the DSpace digital archives until expiry of the term of validity of the copyright,

"Mechanical Characterization of Silver Nanowires",

supervised by Sergei Vlassov,

2. I am aware of the fact that the author retains these rights.

3. I certify that granting the non-exclusive licence does not infringe the intellectual property rights or rights arising from the Personal Data Protection Act.

Tartu, **29.05.2013**